Staggered Turkel–Zwas Schemes for Two-Dimensional Shallow-Water Equations

YUHE SONG

Institute of Marine and Coastal Sciences, Rutgers University, New Brunswick, New Jersey

TAO TANG

Department of Mathematics and Statistics, Simon Fraser University, Burnaby, British Columbia, Canada

(Manuscript received 26 March 1993, in final form 2 July 1993)

ABSTRACT

The Turkel–Zwas-type schemes employ coarse grids to discretize the terms associated with the fast gravity–inertia waves and use fine grids to treat the terms associated with the slow Rossby waves. The ratio of the coarse and fine grids is an integer, $p > 1$, and one can use time steps nearly p times larger than those allowed by the Courant–Friedrich–Lewy condition for the usual explicit leapfrog scheme. This paper investigates the Turkel–Zwas-type schemes with three spatial grids—namely, A (unstaggered), B, and C grids (staggered)—for two-dimensional shallow-water equations. A new method that uses the Laplace transform is introduced to solve the two-dimensional phase solutions. Comparisons of the three grids with coarse and fine-grid resolutions are made. One realistic model problem is tested to verify the linear analysis results. The test shows that the Turkel–Zwas-type schemes can be used for a larger time step in some practical simulations.

1. Introduction

In this paper we consider the application of the transfer function approach to the Turkel–Zwas explicit large-time-step scheme (see Turkel and Zwas 1979) for the two-dimensional shallow-water equations. This scheme employs a coarse grid to discretize the terms associated with the fast gravity–inertia waves but uses a fine grid to treat the terms associated with the slow Rossby waves. The ratio of the coarse and fine grids is an integer, $p > 1$, and one can use time steps nearly p times larger than those allowed by the Courant–Friedrichs–Lewy (CFL) condition for the usual explicit leapfrog scheme (for example, see Navon and de Villiers 1987). The analytical method to be used in this work, that is, the transfer function approach, was introduced by Schoenstadt (1977, 1980) to study the behavior of the semidiscrete one-dimensional shallow-water equations with different finite-difference schemes. As a useful tool in analyzing numerical schemes, the transfer function approach leads to important insights into the differences caused by various discretization schemes, which do not directly emerge from phase propagation considerations alone. Neta and Navon (1989) used this method to analyze the Turkel–Zwas scheme with different values of p for the one-dimensional shallow-water equations. When $p = 1$, various finite-element and finite-difference schemes for the two-dimensional equations were analyzed by Foreman (1984), Neta and DeVito (1988), and Schoenstadt (1980).

Although there have been several applications of the transfer function approach for Turkel–Zwas schemes, most of them have been restricted to unstaggered grid arrangement (for example, see Navon and de Villiers 1987; Neta 1989; Neta and DeVito 1988; Neta and Navon 1989). In general, there are five numerical grids, usually referred to as A–E grids, which are obtained by appropriate arrangements of the dependent variables in the horizontal directions (see, e.g., Arakawa and Lamb 1977). For one-dimensional shallow-water equations, Winninghoff (1968) and Schoenstadt (1980) carried out extensive investigations of geostrophic adjustment for the five grids. Their results suggest that the B grid is the most satisfactory one for the one-dimensional models. For the two-dimensional shallow-water equations Arakawa and Lamb (1977) found that, in contrast to the one-dimensional case, the C grid was the best one among the five grids for fine-grid resolution. The effect of various grid resolutions for these grids has been investigated recently by Wajsowicz (1986) and Neta and Williams (1989). Since the standard Turkel–Zwas scheme uses A grid, we shall refer to the standard Turkel–Zwas scheme as the "T–Z–A" scheme.

In this paper we will extend the T–Z–A scheme to the schemes with B and C grids (i.e., T–Z–B and T–Z–C schemes) and will consider their applications to

Corresponding author address: Dr. T. Tang, Department of Mathematics and Statistics, Simon Fraser University, Burnaby, British Columbia, Canada V5A 1S6.

the two-dimensional shallow-water equations. The reason that we consider only A–C grids is that in practice they are the most useful ones, as was indicated by previous analyses. The main difficulty one will encounter in dealing with the analysis for two-dimensional shallow-water equations is how to solve the two-dimensional phase solutions. Previous techniques to handle the problem have concentrated on the eigenvalue and eigenvector method (see, e.g., Schoenstadt 1980; Neta and Navon 1989), which seems difficult to extend to the two-dimensional models. To overcome the difficulty, Neta (1988) employed the Fourier transform to solve the two-dimensional steady-state phase solutions. In this work we shall show that the use of Laplace transform can easily solve the steady-state part and the transient part of the phase solutions. The stability analysis for these three schemes will be given in the Appendix. One nonlinear model problem will be tested to verify the linear analysis results.

2. Turkel–Zwas schemes

The two-dimensional shallow-water equations in Cartesian coordinates can be written as

$$\frac{\partial u}{\partial t} + u\frac{\partial u}{\partial x} + v\frac{\partial u}{\partial y} + g\frac{\partial h}{\partial x} = fv, \quad (2.1)$$

$$\frac{\partial v}{\partial t} + u\frac{\partial v}{\partial x} + v\frac{\partial v}{\partial y} + g\frac{\partial h}{\partial y} = -fu, \quad (2.2)$$

$$\frac{\partial h}{\partial t} + u\frac{\partial h}{\partial x} + v\frac{\partial h}{\partial y} + h\left(\frac{\partial u}{\partial x} + \frac{\partial v}{\partial y}\right) = 0, \quad (2.3)$$

where u and v are the horizontal components of the perturbation velocity in the x and y directions, respectively, h is the perturbed height of the free surface, g is the acceleration due to gravity, and f is the Coriolis parameter assumed constant in the subsequent analysis. To use the transfer function approach we usually consider the linearized equations with no mean flow in an infinite region (see, e.g., Navon and de Villiers 1987; Neta and Navon 1989; Schoenstadt 1980),

$$\frac{\partial u}{\partial t} - fv + g\frac{\partial h}{\partial x} = 0, \quad (2.4)$$

$$\frac{\partial v}{\partial t} + fu + g\frac{\partial h}{\partial y} = 0, \quad (2.5)$$

$$\frac{\partial h}{\partial t} + H\frac{\partial u}{\partial x} + H\frac{\partial v}{\partial y} = 0, \quad (2.6)$$

where H is the mean height of the free surface. This model is particularly important in the study of the meteorological process called geostrophic adjustment and has been investigated by several researchers (see, e.g., Blumen 1972; Cahn 1945; Neta and Navon 1989; Schoenstadt 1980). Given a positive constant α, $0 \leq \alpha \leq 1$, the Turkel–Zwas-type schemes for (2.4)–(2.6) are T–Z–A (with $q = 2p$):

$$\frac{\partial u_{mn}}{\partial t} = f[(1-\alpha)v_{mn} + \alpha\bar{v}^{p}_{mn}] - \frac{g}{q\Delta x}(h_{m+q/2,n} - h_{m-q/2,n}), \quad (2.7)$$

$$\frac{\partial v_{mn}}{\partial t} = -f[(1-\alpha)u_{mn} + \alpha\bar{u}^{p}_{mn}] - \frac{g}{q\Delta y}(h_{m,n+q/2} - h_{m,n-q/2}), \quad (2.8)$$

$$\frac{\partial h_{mn}}{\partial t} = -\frac{H}{q\Delta x}(u_{m+q/2,n} - u_{m-q/2,n}) - \frac{H}{q\Delta y}(v_{m,n+q/2} - v_{m,n-q/2}); \quad (2.9)$$

T–Z–B (with $q = 2p - 1$):

$$\frac{\partial u_{mn}}{\partial t} = f[(1-\alpha)v_{mn} + \alpha\bar{v}^{p}_{mn}] - \frac{g}{q\Delta x}(\bar{h}^{y}_{m+q/2,n} - \bar{h}^{y}_{m-q/2,n}), \quad (2.10)$$

$$\frac{\partial v_{mn}}{\partial t} = -f[(1-\alpha)u_{mn} + \alpha\bar{u}^{p}_{mn}] - \frac{g}{q\Delta y}(\bar{h}^{x}_{m,n+q/2} - \bar{h}^{x}_{m,n-q/2}), \quad (2.11)$$

$$\frac{\partial h_{mn}}{\partial t} = -\frac{H}{q\Delta x}(\bar{u}^{y}_{m+q/2,n} - \bar{u}^{y}_{m-q/2,n}) - \frac{H}{q\Delta y}(\bar{v}^{x}_{m,n+q/2} - \bar{v}^{x}_{m,n-q/2}); \quad (2.12)$$

T–Z–C (with $q = 2p - 1$):

$$\frac{\partial u_{mn}}{\partial t} = f[(1-\alpha)\bar{v}^{xy}_{mn} + \alpha\bar{v}^{q/2}_{mn}] - \frac{g}{q\Delta x}(h_{m+q/2,n} - h_{m-q/2,n}), \quad (2.13)$$

$$\frac{\partial v_{mn}}{\partial t} = -f[(1-\alpha)\bar{u}^{xy}_{mn} + \alpha\bar{u}^{q/2}_{mn}] - \frac{g}{q\Delta y}(h_{m,n+q/2} - h_{m,n-q/2}), \quad (2.14)$$

$$\frac{\partial h_{mn}}{\partial t} = -\frac{H}{q\Delta x}(u_{m+q/2,n} - u_{m-q/2,n}) - \frac{H}{q\Delta y}(v_{m,n+q/2} - v_{m,n-q/2}), \quad (2.15)$$

where we have set

$$\bar{u}^{y}_{mn} = \frac{1}{2}(u_{m,n+1/2} + u_{m,n-1/2}),$$

$$\bar{u}^{x}_{mn} = \frac{1}{2}(u_{m+1/2,n} + u_{m-1/2,n}),$$

$$\bar{u}^{xy}_{mn} = \frac{1}{4}(u_{m+1/2,n} + u_{m-1/2,n} + u_{m,n+1/2} + u_{m,n-1/2}),$$

$$\bar{u}^{p}_{mn} = \frac{1}{4}(u_{m+p,n} + u_{m-p,n} + u_{m,n+p} + u_{m,n-p}),$$

and similarly for v, and where m and n are the indices of the grid points in the x and y directions, and Δx and Δy are the grid sizes in the x and y directions, respectively. It should be pointed out that the T–Z–A scheme (2.7)–(2.9) is a modified Turkel–Zwas scheme advocated by Neta (1989).

As discussed in Schoenstadt (1977), the linearized shallow-water equations can be solved by using spatial Fourier transforms. Let $\mathbf{w}$ be the vector function

$$\mathbf{w} = (u, v, h)^{\mathrm{T}}, \tag{2.16}$$

where $\mathbf{w}^{\mathrm{T}}$ denotes the transpose of $\mathbf{w}$. The Fourier transform of $\mathbf{w}$ is then given by

$$\hat{\mathbf{w}}(k, l, t) = \int_{-\infty}^{+\infty} \mathbf{w}(x, y, t) \exp[-i(kx + ly)]dxdy.$$

By use of the Fourier transform, (2.4)–(2.6) reduce to

$$\frac{\partial \hat{u}}{\partial t} = f\hat{v} - ikg\hat{h}, \tag{2.17}$$

$$\frac{\partial \hat{v}}{\partial t} = -f\hat{u} - ilg\hat{h}, \tag{2.18}$$

$$\frac{\partial \hat{h}}{\partial t} = -ikH\hat{u} - ilH\hat{v}, \tag{2.19}$$

which can be solved with initial conditions

$$\hat{\mathbf{w}}_0 = \hat{\mathbf{w}}(k, l, 0) = \int_{-\infty}^{+\infty} \mathbf{w}(x, y, 0) \times \exp[-i(kx + ly)]dxdy. \tag{2.20}$$

Similarly, the Fourier transform for the discrete form is

$$\hat{\mathbf{w}}(k, l, t) = \int_{-\infty}^{+\infty} \mathbf{w}(x + \Delta x, y + \Delta y) \times \exp[-i(kx + ly + k\Delta x + l\Delta y)]dxdy.$$

Applying the Fourier transform to (2.7)–(2.15) gives

$$\frac{\partial \hat{u}}{\partial t} = f\rho\hat{v} - ig\xi\hat{h}, \tag{2.21}$$

$$\frac{\partial \hat{v}}{\partial t} = -f\rho\hat{u} - ig\eta\hat{h}, \tag{2.22}$$

$$\frac{\partial \hat{h}}{\partial t} = -iH\xi\hat{u} - iH\eta\hat{v}, \tag{2.23}$$

where ρ, ξ, and η are defined according to different grids; namely,

$$\text{T–Z–A} \quad \rho_A = (1 - \alpha) + \frac{\alpha}{2}(\cos kp\Delta x + \cos lp\Delta y),$$

$$\xi_A = \frac{\sin(kp\Delta x)}{p\Delta x},$$

$$\eta_A = \frac{\sin(lp\Delta y)}{p\Delta y}; \tag{2.24}$$

$$\text{T–Z–B} \quad \rho_B = (1 - \alpha) + \frac{\alpha}{2}(\cos kp\Delta x + \cos lp\Delta y),$$

$$\xi_B = \frac{2\sin(kq\Delta x/2)\cos(l\Delta y/2)}{q\Delta x},$$

$$\eta_B = \frac{2\sin(lq\Delta y/2)\cos(k\Delta x/2)}{q\Delta y}; \tag{2.25}$$

$$\text{T–Z–C} \quad \rho_C = (1 - \alpha)\cos\left(\frac{k\Delta x}{2}\right)\cos\left(\frac{l\Delta y}{2}\right) + \alpha\cos\left(\frac{kq\Delta x}{2}\right)\cos\left(\frac{lq\Delta y}{2}\right),$$

$$\xi_C = \frac{2\sin(kq\Delta x/2)}{q\Delta x},$$

$$\eta_C = \frac{2\sin(lq\Delta y/2)}{q\Delta y}, \tag{2.26}$$

$$\text{continuous} \quad \rho = 1,$$

$$\xi = k,$$

$$\eta = l. \tag{2.27}$$

3. Phase solutions

In this section, we shall solve (2.21)–(2.23) with the initial condition (2.20) by using the Laplace transforms. Let the Laplace transform of $\hat{\mathbf{w}}$ be $\tilde{\mathbf{w}}$; namely,

$$\tilde{\mathbf{w}}(x, y, p) = \mathcal{L}\hat{\mathbf{w}} \equiv \int_0^{\infty} e^{-pt}\hat{\mathbf{w}}(x, y, t)dt. \tag{3.1}$$

Then (2.21)–(2.23) with (2.20) become

$$s\tilde{u} - \hat{u}_0 = f\rho\tilde{v} - i\xi g\tilde{h}, \tag{3.2}$$

$$s\tilde{v} - \hat{v}_0 = -f\rho\tilde{u} - i\eta g\tilde{h}, \tag{3.3}$$

$$s\tilde{h} - \hat{h}_0 = -i\xi H\tilde{u} - i\eta H\tilde{v}. \tag{3.4}$$

Rewriting the preceding equations in a matrix form; that is, $\mathbf{A}\tilde{\mathbf{w}} = \hat{\mathbf{w}}_0$, with

$$\mathbf{A} = \begin{pmatrix} s & -f\rho & i\xi g \\ f\rho & s & i\eta g \\ i\xi H & i\eta H & s \end{pmatrix}, \tag{3.5}$$

we find that the solution of (3.2)–(3.4) is $\tilde{\mathbf{w}} = \mathbf{A}^{-1}\hat{\mathbf{w}}_0$. A direct calculation gives that

$$\mathbf{A}^{-1} = \frac{1}{s(s^2+\omega^2)} \begin{bmatrix} s^2 + gH\eta^2 & sf\rho - gH\xi\eta & -ig(f\rho\eta + s\xi) \\ -(sf\rho + gH\xi\eta) & s^2 + gH\xi^2 & ig(f\rho\xi - s\eta) \\ iH(f\rho\eta - s\xi) & -iH(f\rho\xi + s\eta) & s^2 + (f\rho)^2 \end{bmatrix}, \tag{3.6}$$

where ω is the positive eigenvalue of $\mathbf{A}$,

$$\omega = [(f\rho)^2 + gH(\xi^2 + \eta^2)]^{1/2}. \tag{3.7}$$

The system (2.21)–(2.23) can be solved by using the inverse Laplace transform, and the solution can be formally written as $\hat{\mathbf{w}} = \mathcal{L}^{-1}\tilde{\mathbf{w}} = \mathcal{L}^{-1}[\mathbf{A}^{-1}]\hat{\mathbf{w}}_0$. Noting that

$$\mathcal{L}^{-1}\left[\frac{1}{s^2+\omega^2}\right] = \frac{\sin\omega t}{\omega}, \quad \mathcal{L}^{-1}\left[\frac{s}{s^2+\omega^2}\right] = \cos\omega t,$$

$$\mathcal{L}^{-1}\left[\frac{1}{s}\right] = 1, \quad \mathcal{L}^{-1}\left[\frac{1}{s(s^2+\omega^2)}\right] = \frac{1-\cos\omega t}{\omega^2},$$

we obtain from (3.6) that

$$\mathcal{L}^{-1}(\mathbf{A}^{-1}) = \begin{bmatrix} \cos\omega t + gH\eta^2 S & f\rho\dfrac{\sin\omega t}{\omega} - gH\xi\eta S & -ig\xi\dfrac{\sin\omega t}{\omega} - igf\rho\eta S \\ -f\rho\dfrac{\sin\omega t}{\omega} - gH\xi\eta S & \cos\omega t + gH\xi^2 S & -ig\eta\dfrac{\sin\omega t}{\omega} + igf\rho\xi S \\ -iH\xi\dfrac{\sin\omega t}{\omega} + iHf\rho\eta S & -iH\eta\dfrac{\sin\omega t}{\omega} - iHf\rho\xi S & \cos\omega t + (f\rho)^2 S \end{bmatrix},$$

where $S = (1 - \cos\omega t)/\omega^2$. The solutions of (2.21)–(2.23) are

$$\begin{pmatrix} \hat{u} \\ \hat{v} \\ \hat{h} \end{pmatrix} = \mathcal{L}^{-1}[\mathbf{A}^{-1}] \begin{pmatrix} \hat{u}_0 \\ \hat{v}_0 \\ \hat{h}_0 \end{pmatrix}. \tag{3.8}$$

It is known that each transform field can be written as the sum of a steady-state part (denoted by s subscript) and a transient part; see Haltiner and Williams (1980). In the present case the steady part is

$$\begin{pmatrix} \hat{u}_s \\ \hat{v}_s \\ \hat{h}_s \end{pmatrix} = \begin{pmatrix} \dfrac{gH\eta^2}{\omega^2} & -\dfrac{gH\xi\eta}{\omega^2} & -\dfrac{igf\rho\eta}{\omega^2} \\ -\dfrac{gH\xi\eta}{\omega^2} & \dfrac{gH\xi^2}{\omega^2} & \dfrac{igf\rho\xi}{\omega^2} \\ \dfrac{iHf\rho\eta}{\omega^2} & -\dfrac{iHf\rho\xi}{\omega^2} & \dfrac{(f\rho)^2}{\omega^2} \end{pmatrix} \begin{pmatrix} \hat{u}_0 \\ \hat{v}_0 \\ \hat{h}_0 \end{pmatrix}. \tag{3.9}$$

Similarly, we can find that the steady-state solution in the continuous case is

$$\begin{pmatrix} \hat{u}_s \\ \hat{v}_s \\ \hat{h}_s \end{pmatrix} = \begin{pmatrix} \dfrac{gHl^2}{\omega^2} & -\dfrac{gHkl}{\omega^2} & -\dfrac{igfl}{\omega^2} \\ -\dfrac{gHkl}{\omega^2} & \dfrac{gHk^2}{\omega^2} & \dfrac{igfk}{\omega^2} \\ \dfrac{iHfl}{\omega^2} & -\dfrac{iHfk}{\omega^2} & \dfrac{f^2}{\omega^2} \end{pmatrix} \begin{pmatrix} \hat{u}_0 \\ \hat{v}_0 \\ \hat{h}_0 \end{pmatrix}. \tag{3.10}$$

The preceding steady solutions were also obtained by Neta (1988) using Fourier transforms.

4. Numerical comparisons

Throughout this section the parameter α in (2.7)–(2.15) is set to be 1/3. Before presenting the numerical results, we shall introduce some physical parameters that will be used in the following. The Rossby radius of deformation is basically the horizontal scale at which rotation effects become as important as buoyancy in the rotating fluid called "atmosphere." For the atmosphere the Rossby radius of deformation is defined as

$$\lambda = \frac{(gh)^{1/2}}{f} \approx \frac{(9.8 \times 10^2)^{1/2}}{10^{-4}} \approx 3.13 \times 10^5 \text{ m}, \tag{4.1}$$

where g is the acceleration of gravity and h is the depth of the fluid. Wavenumbers in the x and y directions, k and l, are defined in the region

$$-\frac{\pi}{d} < k < \frac{\pi}{d}, \quad -\frac{\pi}{d} < l < \frac{\pi}{d}, \tag{4.2}$$

where $d = \Delta x = \Delta y$. (Here, without loss of generality we assume that a square grid is used.) The ratio of the grid size to Rossby radius of deformation, $R = d/\lambda$, called "grid resolution," plays an important role in the present problem. Since the Rossby radius is fixed [see (4.1)], a small ratio corresponds to a small-scale length while a large ratio corresponds to a large-scale length.

Dispersion is the interference of Fourier modes that comes about if the wavenumbers k and l and the frequency ω [see (3.7)] are related nonlinearly. In general, the dispersion relation for a partial differential equation is a polynomial in k and l, while a discrete model amounts to a trigonometric approximation. It has been noted that even if the CFL condition is satisfied, numerical schemes may be unstable due to the dispersion (see, e.g., Trefethen 1982). The analytic and discrete dispersion relations are given by (3.7) and (2.24)–(2.27). Figure 1 shows a comparison of the dependence of ω/f in $(kd/\pi, ld/\pi) \in [0, 1] \times [0, 1]$ for the case $R = 0.5$. This figure contains the analytic solution and the numerical solutions for $p = 1$, 2, and 3. It can be seen from Fig. 1 that, in the case $p = 1$, T–Z–C is clearly better than T–Z–A and T–Z–B when compared with the analytic solution, which is in good agreement with Arakawa and Lamb (1977). When $p = 2$ and 3, Fig. 1 suggests that T–Z–B is better than T–Z–C in the sense that the contour curves given by T–Z–B are closer to the analytic solution than those obtained by T–Z–C. Moreover, it is observed from Fig. 1 that T–Z–C is slightly better than T–Z–A. Figure 2 gives a comparison of ω/f for the case $R = 2$, which corresponds to a coarse-grid resolution. For this case, T–Z–C is clearly worse than the A and B grids, even when $p = 1$. Figure 2 also indicates that T–Z–B is better than T–Z–A.

Furthermore, we compare the height fields for the continuous and the discrete models, using the same methodology as in Arakawa and Lamb (1977) and Schoenstadt (1980). An initial distribution given by

$$u_0(x, y, 0) = 0,$$
$$v_0(x, y, 0) = \begin{cases} V_0, & -d < x, \quad y < d, \\ 0, & \text{otherwise}, \end{cases}$$
$$h_0(x, y, 0) = 0, \tag{4.3}$$

is considered. Transforming the preceding functions into the phase space gives

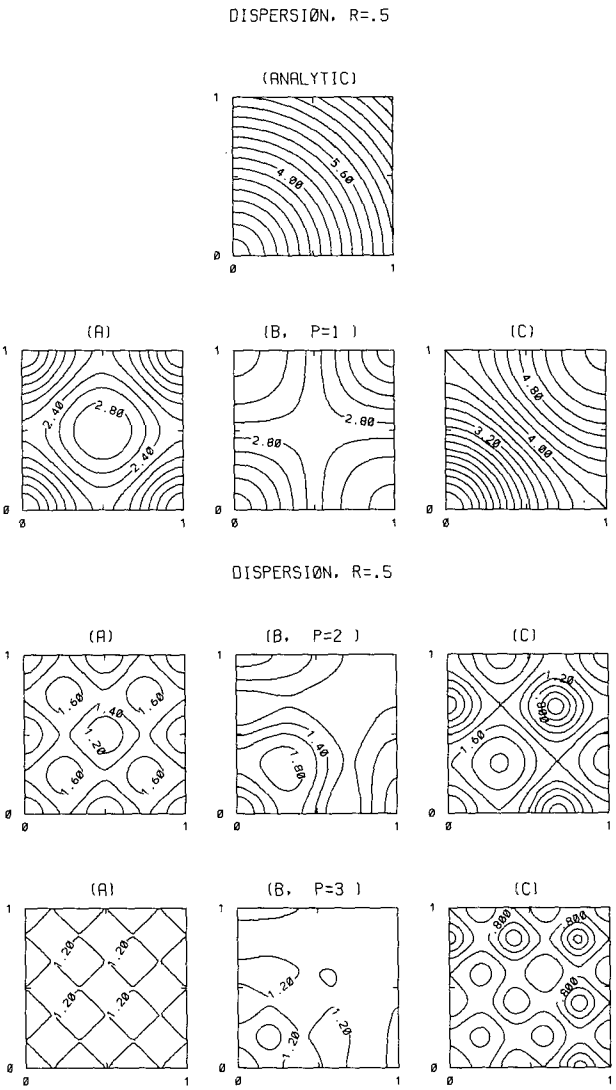

FIG 1. Contours of ω/f as a function of kd/π and ld/π for $R = 0.5$. The first row gives the analytic solution. The second to fourth rows are numerical solutions using the Turkel–Zwas scheme with A, B, and C grids with $p = 1$, 2, and 3, respectively.

$$\hat{u}_0 = 0,$$
$$\hat{v}_0 = 4V_0 \frac{\sin(\xi d)}{\xi} \frac{\sin(\eta d)}{\eta},$$
$$\hat{h}_0 = 0.$$

Substituting the foregoing equations into (3.8) gives

$$\hat{h} = -4iHV_0\left[\frac{\eta \sin\omega t}{\omega} + \frac{f\rho\xi(1 - \cos\omega t)}{\omega^2}\right] \times \frac{\sin\xi d}{\xi} \frac{\sin\eta d}{\eta}. \tag{4.4}$$

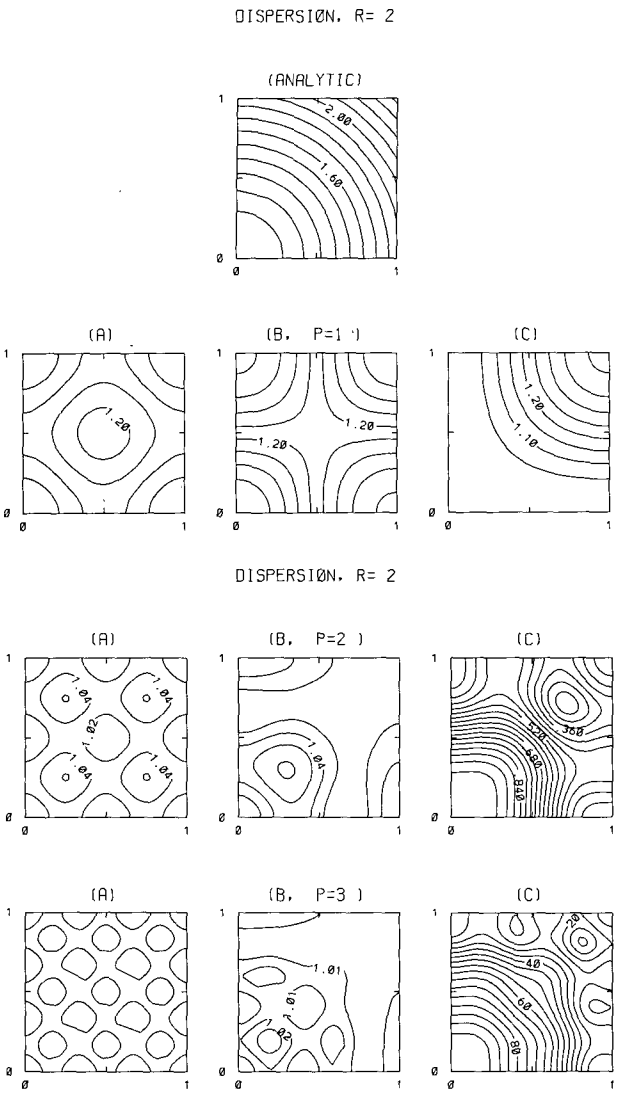

FIG. 2. Same as Fig. 1 except that $R = 2$.

We obtain from (4.4) that

$$h = \frac{V_0 H}{\pi^2} \int_{-\pi/d}^{\pi/d} \int_{-\pi/d}^{\pi/d} \left[\frac{\eta \sin\omega t}{\omega} + \frac{f\rho\xi(1 - \cos\omega t)}{\omega^2} \right] \times \frac{\sin\xi d}{\xi} \frac{\sin\eta d}{\eta} \sin(\xi x + \eta y) d\xi d\eta, \quad (4.5)$$

where η, ξ, ρ, and ω are given in section 2 for the schemes T–Z–A, T–Z–B, T–Z–C, and the continuous case. Specially, in the continuous case ($\rho = 1$, $\xi = k$, and $\eta = l$), we have

$$h = \frac{V_0 H}{\pi^2} \int_{-\pi/d}^{\pi/d} \int_{-\pi/d}^{\pi/d} \left[\frac{l \sin\omega t}{\omega} + \frac{fk(1 - \cos\omega t)}{\omega^2} \right] \times \frac{\sin kd}{k} \frac{\sin ld}{l} \sin(kx + ly) dk dl. \quad (4.6)$$

We have calculated h by using the Simpson's quadrature rule in the region $[0, \pi/d] \times [0, \pi/d]$, with 200 grid points in each direction. The height fields at the corner point $x = y = d$ are plotted for $p = 1$, 2, and 3 in the time period of 80 h. It can be seen from Figs. 3 and 4 that, when $p = 1$, T–Z–C is the most accurate approximation to the analytic solution. Figure 3 shows that for the case $R = 0.5$, the solutions of the A grid are less accurate than those obtained by T–Z–B and T–Z–C. For the coarse-grid resolution, as shown in Fig. 4, T–Z–C is clearly worse than T–Z–A and T–Z–B when $p > 1$.

The preceding results lead to the following comparison results:

$$p > 1, R = 0.5$$
$$\text{T–Z–B} \prec \text{T–Z–C} \prec \text{T–Z–A}$$

$$p > 1, R = 2$$
$$\text{T–Z–B} \prec \text{T–Z–A} \prec \text{T–Z–C}.$$

The "$\prec$" symbol stands for superiority. In particular, we find from the linear analysis that if the grid size is smaller than the Rossby radius of deformation, then the unstaggered grid, T–Z–A, is less appropriate than the staggered B and C grids. This will be verified in the next section by considering a realistic problem.

5. A realistic model problem

In this section we shall apply the Turkel–Zwas schemes to a realistic model. Over recent years there has been a great interest in modeling California coastal flow because of its importance to societal implications and its computational difficulty of complex geometry. The complex geometry, especially the steep topography, severely restricted the time step by the CFL condition in numerical simulation. It is advantageous to use the Turkel–Zwas schemes so that a larger time step can be used.

The region we shall be concerned with is an irregular domain of approximately 1000 km in along-channel length and 700 km in cross-shelf extent; see Fig. 5. The coastal wall is irregular in shape, featuring a set of capes and bays. The underlying bottom topography is smoothed from the realistic region with minimum depth value of 90 m near the coastline and maximum depth value of 4600 m in the deep adjacent ocean. The computational domain is discretized into 98×65 grid cells and maps to the physical domain by the orthogonal coordinate transformation

$$(ds)_\xi = \left(\frac{1}{m}\right) d\xi, \quad (5.1)$$

$$(ds)_\eta = \left(\frac{1}{n}\right) d\eta, \quad (5.2)$$

where ξ and η are the eastward and northward coordinates, respectively, and $m(\xi, \eta)$ and

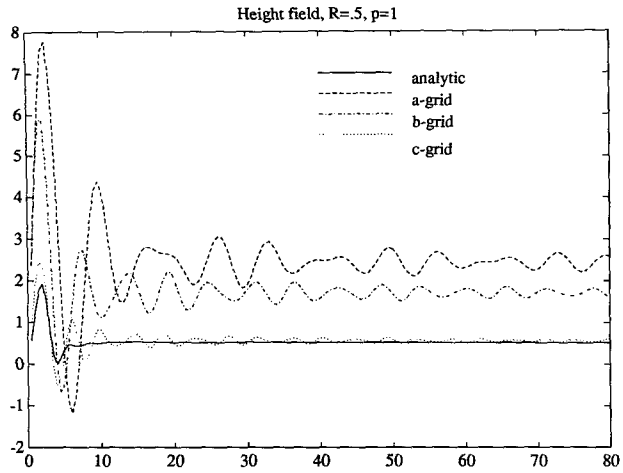

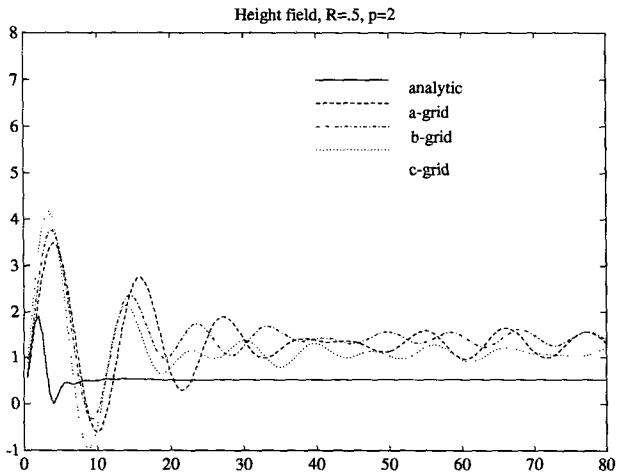

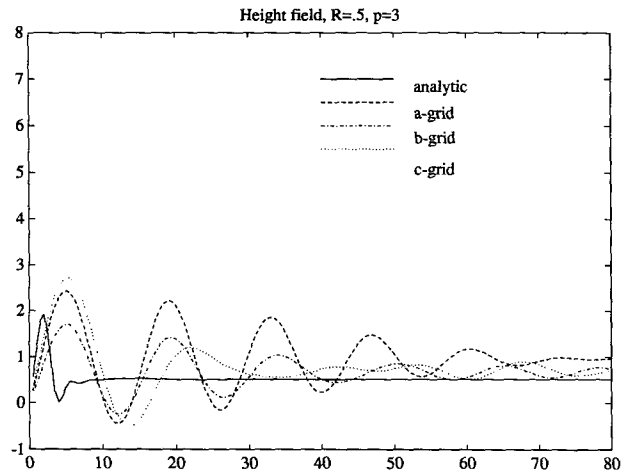

FIG. 3. Time variation of the height perturbation at $x = y = d$ for the shallow-water equations with the initial condition Eq. (4.3) for $R = 0.5$: (a) $p = 1$, (b) $p = 2$, and (c) $p = 3$.

$n(\xi, \eta)$ are the scale factors that relate the differential distances $(\Delta\xi, \Delta\eta)$ to the actual (physical) arc lengths.

Under this horizontal curvilinear coordinate system, the shallow-water equations can be written as [see, e.g., Arakawa and Lamb (1977)]

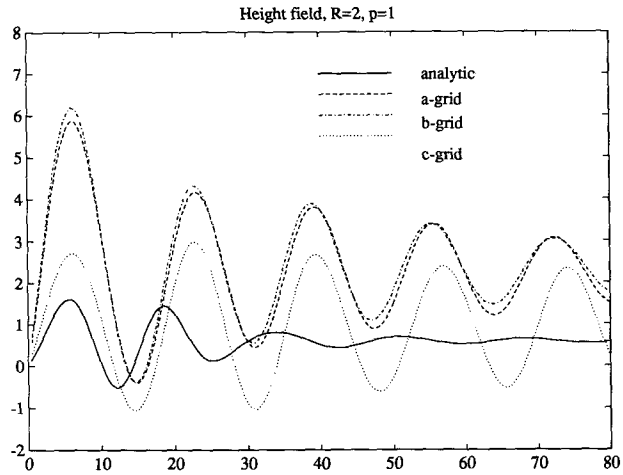

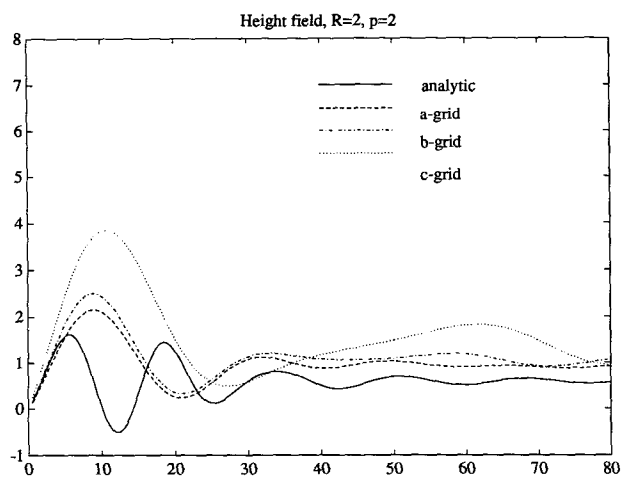

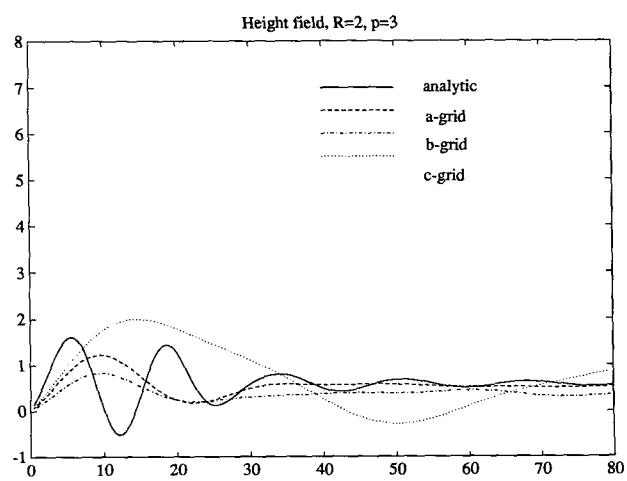

FIG. 4. Same as Fig. 3 except that $R = 2$.

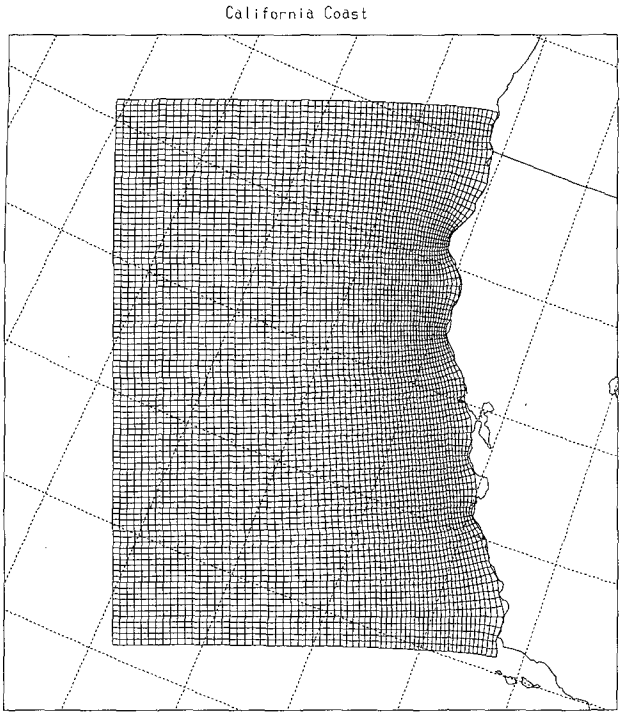

FIG. 5. California coastal region and curvilinear grid.

$$\frac{\partial}{\partial t}\left(\frac{Hu}{mn}\right) = \left(\frac{f}{mn} + v\frac{\partial}{\partial \xi}\frac{1}{n} - u\frac{\partial}{\partial \eta}\frac{1}{m}\right)Hv - \frac{H}{n}\frac{\partial h}{\partial \xi} - \left[\frac{\partial}{\partial \xi}\left(\frac{Hu}{n}u\right) + \frac{\partial}{\partial \eta}\left(\frac{Hv}{m}u\right)\right] + \frac{H}{mn}\mathcal{D}_u + \frac{\tau_\xi}{mn}, \quad (5.3)$$

$$\frac{\partial}{\partial t}\left(\frac{Hv}{mn}\right) = -\left(\frac{f}{mn} + v\frac{\partial}{\partial \xi}\frac{1}{n} - u\frac{\partial}{\partial \eta}\frac{1}{m}\right)Hu - \frac{H}{m}\frac{\partial h}{\partial \eta} - \left[\frac{\partial}{\partial \xi}\left(\frac{Hu}{n}v\right) + \frac{\partial}{\partial \eta}\left(\frac{Hv}{m}v\right)\right] + \frac{H}{mn}\mathcal{D}_v + \frac{\tau_\eta}{mn}, \quad (5.4)$$

$$\frac{\partial}{\partial t}\left(\frac{h}{mn}\right) + \frac{\partial}{\partial \xi}\left(H\frac{u}{n}\right) + \frac{\partial}{\partial \eta}\left(H\frac{v}{m}\right) = 0, \quad (5.5)$$

where $\mathcal{D}_u$ and $\mathcal{D}_v$ are the diffusive terms, and τ_ξ and τ_η are the components of wind stress acting on the surface in the ξ and η directions, respectively. The driving force is provided by an along-coastal equatorward wind,

$$\tau_\xi = 0, \quad \tau_\eta = -\sin\left(\frac{\pi\eta}{L_\xi}\right)(\text{dyn cm}^{-2}),$$

where L_ξ is the width of the computational domain.

The equations (5.3)–(5.5) are discretized by use of the Turkel–Zwas-type schemes as described in section 2. We use a leapfrog scheme for the time integration. The coastal wall and the offshore boundary are treated as closed boundaries. The flow is periodic in the along-coastal direction. The orthogonal curvilinear grid, generated by a software package developed by Wilkin and Hedström (1991, personal communication), is shown in Fig. 5. With this grid, the CFL conditions with C grid can be calculated by (A.17) in the Appendix. The contours of the CFL condition as a function of the depth H and grid size $\Delta\xi$ for T–Z–C with $p = 1$ are plotted in Fig. 6. It is observed from Fig. 6 that the minimum time step allowed is 17.5 s, while the maximum is about 142.5 s. This implies that the time step is severely restricted by the CFL condition in the interior deep ocean where the depth H is about 4600 m. By a simple calculation we can see that the minimum value 17.5 s comes from

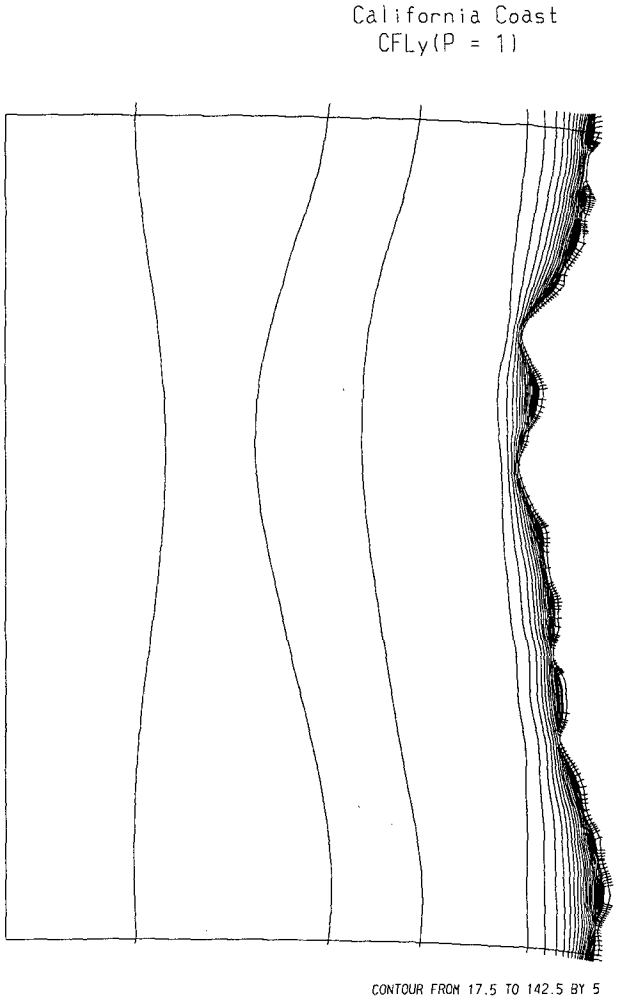

FIG. 6. Contours of the CFL condition as a function of the depth H and grid size $\Delta\xi$ for the T–Z–C scheme with $p = 1$.

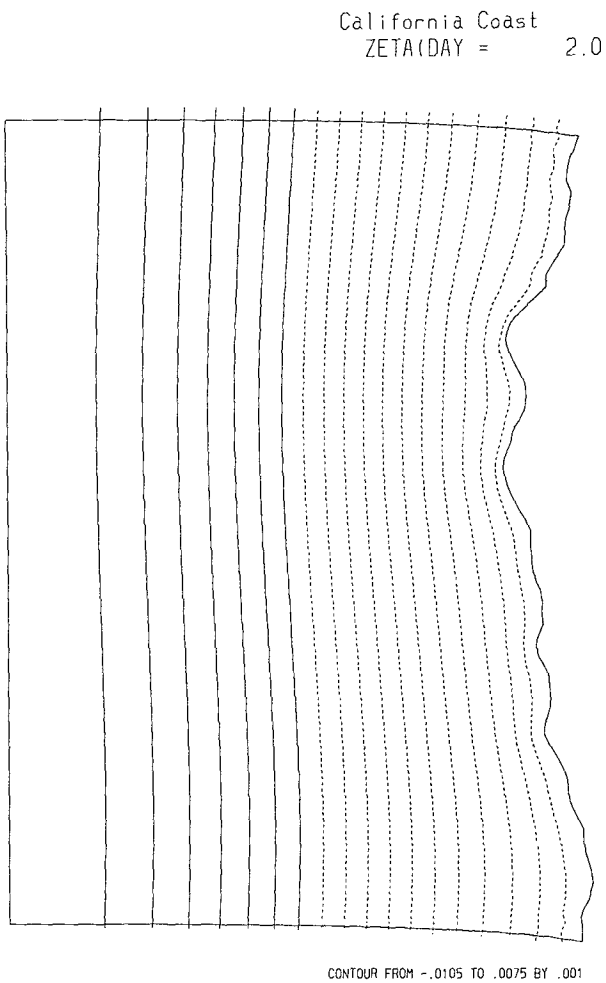

FIG. 7. Contours of height perturbation h calculated by T–Z–C with $p = 2$ after 2 days. Solid and dashed lines stand for above and below rest sea level, respectively.

$$\frac{\Delta\xi}{2(2gH)^{1/2}} \approx \frac{70\,000/65}{2(2 \times 9.8 \times 4600)^{1/2}} \approx 17.5 \text{ s.}$$

Therefore, the Turkel–Zwas-type schemes need only to be used in the interior ocean where boundary conditions can be avoided.

On the other hand, we notice that the grid size $\Delta\xi \approx 1.1 \times 10^4$, which is less than the Rossby radius of deformation; see (4.1). In other words, we are using a fine-grid resolution; that is, $R < 1$. The linear analysis carried out in the last section suggests that in this case the unstaggered Turkel–Zwas scheme T–Z–A is not as good as the T–Z–B and T–Z–C schemes. This is confirmed by our numerical experiments. For example, we find that with T–Z–B and T–Z–C a time step Δt of 24 s can be used to obtain stable numerical solutions up to 48 h. To see this we plot the contours of the perturbed height and velocity field obtained using the T–Z–C scheme with $p = 2$ and $\Delta t = 24$ s in Figs. 7 and 8. It is seen from Figs. 7 and 8 that smooth results for the perturbed height and the velocity are obtained. However, the T–Z–A scheme with the same values of p and Δt produces noisy solutions even after only 12 h. Although the calculated velocity field (see Fig. 9) seems reasonably smooth, unstable results for the perturbed height are observed in Fig. 10. This suggests that in order to obtain stable solutions up to two days with the unstaggered Turkel–Zwas scheme, a smaller time step than that allowed by T–Z–B and T–Z–C should be employed. This is due to the following two reasons. First, as mentioned in the last section, even if the CFL condition is satisfied, numerical schemes may be unstable due to the dispersion. It is seen in the last section that the dispersion error of the T–Z–A scheme is larger than that of the T–Z–B and T–Z–C schemes for the case $R < 1$. Next, in the case when the curvilinear coordinates are used the metric coefficients $m(\xi, \eta)$ and $n(\xi, \eta)$ cannot be evaluated analytically. The staggered schemes average the metric coefficients $m(\xi, \eta)$ and $n(\xi, \eta)$, especially when $p > 1$, which enables us

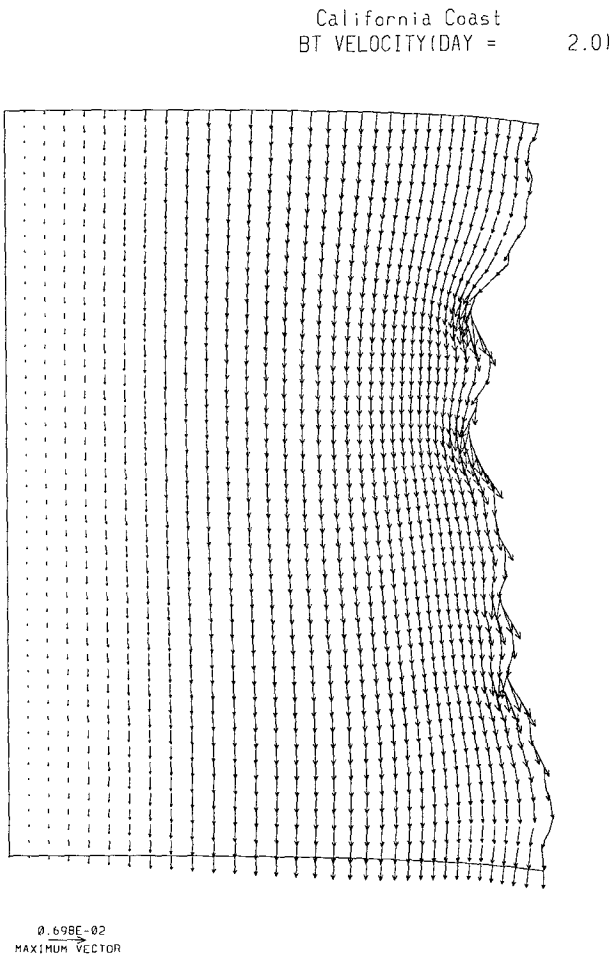

FIG. 8. Velocity field calculated by T–Z–C with $p = 2$ after 2 days.

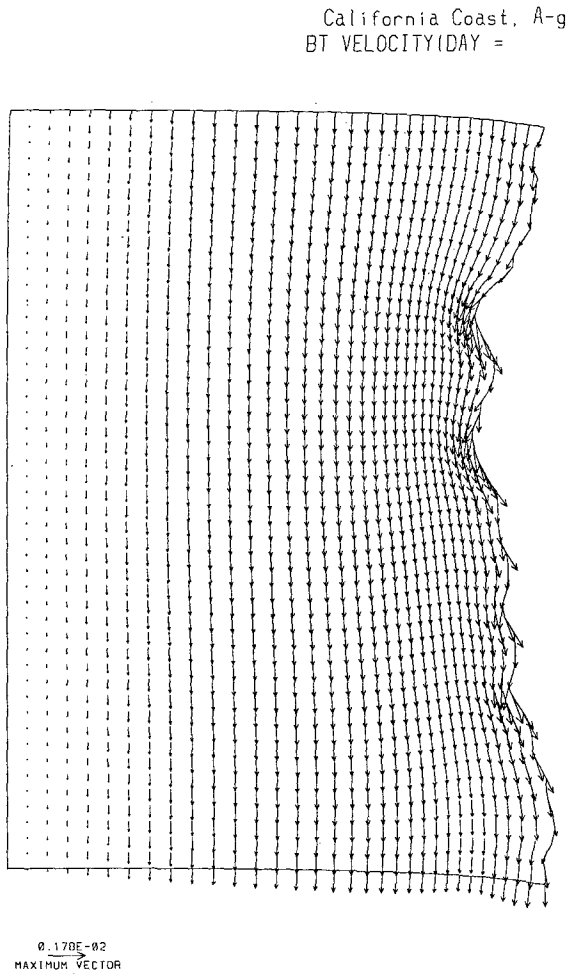

FIG. 9. Velocity field calculated by T–Z–A with $p = 2$ after 0.5 days.

to obtain smoother results. It should be pointed out that if $m(\xi, \eta)$ and $n(\xi, \eta)$ can be calculated analytically, which is the case when spherical coordinates are used, the T–Z–A scheme may produce reasonable results (see Navon and Yu 1991).

The numerical calculations also suggest that in order to obtain smooth solutions up to 48 h, the largest time steps that can be used for the T–Z–C scheme with $p = 1$, 2, and 3 are 16, 24, and 28 s, respectively, which are less than those predicted by (A.17). One of the reasons is again due to the dispersion. In particular, although the Turkel–Zwas-type schemes with $p > 3$ allow large time steps they are not suitable in practical calculations due to unacceptable dispersion errors (see Figs. 1 and 2). Moreover, the CFL condition (A.17) is obtained by assuming that the solution domain is infinite. In the case that a finite domain is used, only half side of the derivatives on the boundary is imposed when the Turkel–Zwas-type schemes are used. This also yields smaller time steps in practical calculations.

6. Conclusions

In this work, we have extended the standard Turkel–Zwas scheme to staggered schemes that use B and C grids. The transfer function approach has been applied to the Turkel–Zwas-type schemes for the two-dimensional shallow-water equations. The two-dimensional phase solutions are solved by using the Laplace transform. The linear analysis and a realistic problem suggest that for $p > 1$ the staggered Turkel–Zwas schemes, T–Z–B and T–Z–C, are more appropriate than the unstaggered Turkel–Zwas scheme if the numerical grid size is smaller than the Rossby radius of deformation. The linear analysis also suggests that if the numerical grid size is greater than the Rossby radius, then T–Z–B is more appropriate than T–Z–A, and T–Z–A is more appropriate than T–Z–C.

The main advantage of the standard Turkel–Zwas scheme is that it allows time steps nearly p times larger than those given by the CFL condition for the usual explicit leapfrog scheme. It can be seen from the Ap-

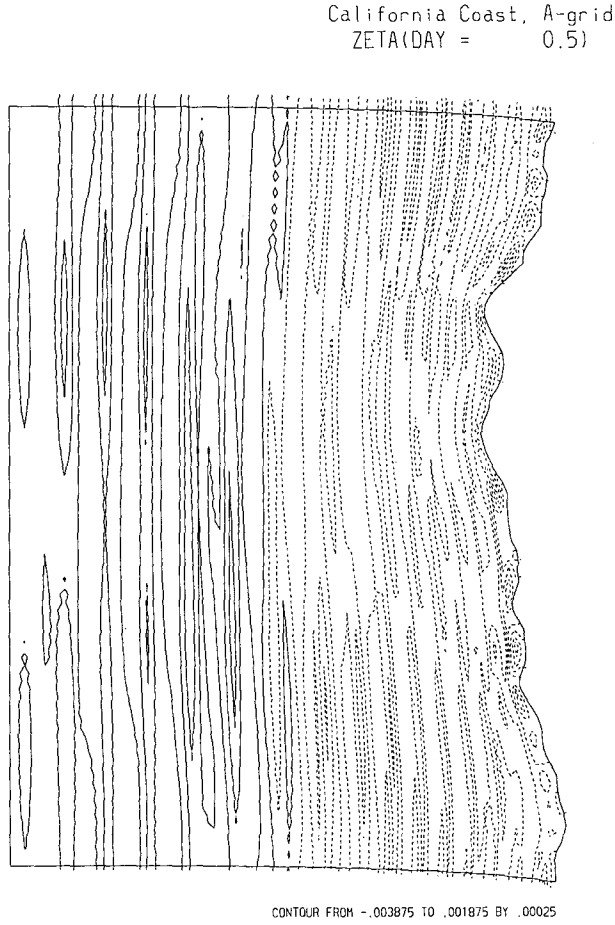

FIG. 10. Contours of height perturbation h calculated by T–Z–A with $p = 2$ after 0.5 days. Solid and dashed lines stand for above and below rest sea level, respectively.

pendix that when p becomes larger the time steps allowed by T–Z–B and T–Z–C are nearly the same as those given by T–Z–A. In other words, the staggered Turkel–Zwas schemes preserve the main advantage of the standard Turkel–Zwas scheme. One nonlinear model problem is tested to verify the linear analysis results. The test shows that the Turkel–Zwas-type schemes can be used for a larger time step in some practical simulations.

Further research is to investigate conservation of three discretized integral invariants for the staggered Turkel–Zwas schemes—that is, the conservation of total mass, total energy, and potential enstrophy. As was suggested by Navon and de Villiers (1987), these properties are important for long-term integrations and medium-range forecasts.

Acknowledgments. We are grateful to Professor I. M. Navon and the referees for many helpful comments and suggestions that have improved the presentation and content of this paper. This research was supported under Natural Sciences and Engineering Research Council of Canada Grant OGP0105545.

APPENDIX

Stability Analysis

For the sake of simplicity, we set $f = 0$ in (2.1)–(2.3). In the stability analysis we usually consider constant coefficients; that is, the coefficients u, v, and h are replaced by u_0, v_0, and h_0, respectively. Using the vector notation (2.16), we write (2.1)–(2.3) into the following matrix form:

$$-\frac{\partial \mathbf{w}}{\partial t} = \begin{pmatrix} u_0 & 0 & g \\ 0 & u_0 & 0 \\ h_0 & 0 & u_0 \end{pmatrix} \frac{\partial \mathbf{w}}{\partial x} + \begin{pmatrix} v_0 & 0 & 0 \\ 0 & v_0 & g \\ 0 & h_0 & v_0 \end{pmatrix} \frac{\partial \mathbf{w}}{\partial y}. \tag{A.1}$$

Setting

$$\mathbf{z} = \begin{pmatrix} \sqrt{h_0} & 0 & 0 \\ 0 & \sqrt{h_0} & 0 \\ 0 & 0 & \sqrt{g} \end{pmatrix} \mathbf{w}, \tag{A.2}$$

we obtain from (A.1) that

$$-\frac{\partial \mathbf{z}}{\partial t} = \mathbf{G}[\mathbf{z}], \tag{A.3}$$

where the operator $\mathbf{G}$ is defined by

$$\mathbf{G} = \begin{pmatrix} u_0 & 0 & \sqrt{gh_0} \\ 0 & u_0 & 0 \\ \sqrt{gh_0} & 0 & u_0 \end{pmatrix} \frac{\partial}{\partial x} + \begin{pmatrix} v_0 & 0 & 0 \\ 0 & v_0 & \sqrt{gh_0} \\ 0 & \sqrt{gh_0} & v_0 \end{pmatrix} \frac{\partial}{\partial y}. \tag{A.4}$$

Consider the leapfrog scheme for (A.3):

$$\mathbf{z}^{k+1} = \mathbf{z}^{k-1} - 2\Delta t \mathbf{G}^*[\mathbf{z}^k], \tag{A.5}$$

where $\mathbf{G}^*$ is a discretized approximation for $\mathbf{G}$. The stability condition for (A.5) is equivalent to that for

$$\mathbf{z}^{k+1} = \mathbf{z}^k - \Delta t \mathbf{G}^*[\mathbf{z}^k], \tag{A.6}$$

since (A.5) can be split into (A.6) and a backward Euler scheme that has no stability restriction. Therefore, the stability condition for (A.6) is

$$\Delta t \|\mathbf{G}^*\| < 1, \tag{A.7}$$

where $\| \quad \|$ is a norm. For convenience, the norm in (A.7) is chosen as the l_2 norm. We define the following difference operators to approximate $\partial/\partial x$:

$$\delta_x^p u_m = \frac{u_{m+p} - u_{m-p}}{2pd},$$

$$\bar{\delta}_{px}^{\,y} u_m = \frac{\bar{u}^y_{m+q/2} - \bar{u}^y_{m-q/2}}{qd},$$

$$\delta_{px} u_m = \frac{u_{m+q/2} - u_{m-q/2}}{qd},$$

where $q = 2p - 1$. Approximations for $\partial/\partial y$ can be defined in a similar way. Using the preceding notations we obtain the forms for $\mathbf{G}^*$ with respect to T–Z–A, T–Z–B, and T–Z–C as

T–Z–A:
$$\begin{pmatrix} u_0\delta_x^1 + v_0\delta_y^1 & 0 & \sqrt{gh_0}\,\delta_x^p \\ 0 & u_0\delta_x^1 + v_0\delta_y^1 & \sqrt{gh_0}\,\delta_y^p \\ \sqrt{gh_0}\,\delta_x^p & \sqrt{gh_0}\,\delta_y^p & u_0\delta_x^1 + v_0\delta_y^1 \end{pmatrix};$$

T–Z–B:
$$\begin{pmatrix} u_0\bar{\delta}_{1x}^{\,y} + v_0\bar{\delta}_{1y}^{\,x} & 0 & \sqrt{gh_0}\,\bar{\delta}_{px}^{\,y} \\ 0 & u_0\bar{\delta}_{1x}^{\,y} + v_0\bar{\delta}_{1y}^{\,x} & \sqrt{gh_0}\,\bar{\delta}_{py}^{\,x} \\ \sqrt{gh_0}\,\bar{\delta}_{px}^{\,y} & \sqrt{gh_0}\,\bar{\delta}_{py}^{\,x} & u_0\bar{\delta}_{1x}^{\,y} + v_0\bar{\delta}_{1y}^{\,x} \end{pmatrix};$$

T–Z–C:
$$\begin{pmatrix} u_0\delta_{1x} + v_0\delta_{1y} & 0 & \sqrt{gh_0}\,\delta_{px} \\ 0 & u_0\delta_{1x} + v_0\delta_{1y} & \sqrt{gh_0}\,\delta_{py} \\ \sqrt{gh_0}\,\delta_{px} & \sqrt{gh}\,\delta_{py} & u_0\delta_{1x} + v_0\delta_{1y} \end{pmatrix},$$

TABLE A1. Parameters α_p and β_p.

	α_p	β_p
T–Z–A	$\dfrac{i\sin(pkd)}{pd}$	$\dfrac{i\sin(pld)}{pd}$
T–Z–B	$\dfrac{i\sin[(p-1/2)kd]\cos(ld/2)}{(p-1/2)d}$	$\dfrac{i\sin[(p-1/2)ld]\cos(kd/2)}{(p-1/2)d}$
T–Z–C	$\dfrac{i\sin[(p-1/2)kd]}{(p-1/2)d}$	$\dfrac{i\sin[(p-1/2)ld]}{(p-1/2)d}$

where coarse grids are employed to discretize the terms associated with the fast gravity–inertia waves, and fine grids are used to deal with the slow Rossby wave terms. Taking Fourier transform for G^* gives

$$\hat{\mathbf{G}}^* = \mathcal{F}\mathbf{G}^* = \begin{pmatrix} u_0\alpha_1 + v_0\beta_1 & 0 & \sqrt{gh_0}\alpha_p \\ 0 & u_0\alpha_1 + v_0\beta_1 & \sqrt{gh_0}\beta_p \\ \sqrt{gh_0}\alpha_p & \sqrt{gh_0}\beta_p & u_0\alpha_1 + v_0\beta_1 \end{pmatrix}, \tag{A.8}$$

where α_p and β_p correspond to the Fourier transforms of the difference operators in the x and y directions, respectively. The eigenvalues of $\hat{\mathbf{G}}^*$ are

$$\lambda_0 = u_0\alpha_1 + v_0\beta_1, \tag{A.9}$$

$$\lambda_{\pm 1} = u_0\alpha_1 + v_0\beta_1 \pm [gh_0(\alpha_p^2 + \beta_p^2)]^{1/2}. \tag{A.10}$$

This leads to

$$\|\hat{\mathbf{G}}^*\| \leqslant |u_0\alpha_1| + |v_0\beta_1| + [gh_0(\alpha_p^2 + \beta_p^2)]^{1/2}. \tag{A.11}$$

The parameters α_p and β_p are listed in Table A1.

Using Table A1, together with (A.7) and (A.11), gives the following stability conditions:

$$\text{T–Z–A:} \quad \frac{\Delta t}{d} < \frac{p}{p|u_0| + p|v_0| + (2gh_0)^{1/2}}, \tag{A.12}$$

$$\text{T–Z–B:} \quad \frac{\Delta t}{d} < \frac{p - 1/2}{q|u_0 \sin q\theta| + q|v_0 \cos\theta| + [gh_0(\sin^2 q\theta + \cos^2\theta)]^{1/2}}, \tag{A.13}$$

$$\text{T–Z–C:} \quad \frac{\Delta t}{d} < \frac{p - 1/2}{(2p-1)|u_0| + (2p-1)|v_0| + (2gh_0)^{1/2}}, \tag{A.14}$$

where in (A.13) $q = 2p - 1$ and $\theta = kd/2$. Since $|u_0| + |v_0| \ll (gh_0)^{1/2}$, the following simple stability conditions are obtained:

$$\text{T–Z–A:} \quad \frac{\Delta t}{d} < \frac{p}{(2gh_0)^{1/2}}, \tag{A.15}$$

$$\text{T–Z–B:} \quad \frac{\Delta t}{d} < \frac{p - 1/2}{[gh_0(\sin^2 q\theta + \cos^2\theta)]^{1/2}}, \tag{A.16}$$

$$\text{T–Z–C:} \quad \frac{\Delta t}{d} < \frac{p - 1/2}{(2gh_0)^{1/2}}. \tag{A.17}$$

It can be observed from (A.15)–(A.17) that for larger values of p the stability conditions of T–Z–B and T–Z–C are nearly same as that of T–Z–A.

REFERENCES

Arakawa, A., and V. R. Lamb, 1977: Computational design of the basic dynamical process of the U.C.L.A. general circulation model. *Methods in Computational Physics,* Vol. 17, Academic Press, 174–265.

Blumen, W., 1972: Geostrophic adjustment. *Rev. Geophys. Space Phys.*, **10,** 485–528.

Cahn, A., 1945: An investigation of the free oscillations of a simple current system. *J. Meteor.*, **2,** 113–119.

Foreman, M. G. G., 1984: A two-dimensional dispersion analysis of selected methods for solving the linearized shallow-water equations. *J. Comput. Phys.*, **56,** 287–323.

Haltiner, G. J., and R. T. Williams, 1980: *Numerical Prediction and Dynamic Meteorology.* Wiley and Sons, 477 pp.

Navon, I. M., and R. de Villiers, 1987: The application of the Turkel–Zwas explicit large time-step scheme to a hemispheric barotropic model with constraint restoration. *Mon. Wea. Rev.*, **115,** 1036–1051.

——, and J. Yu, 1991: EXSHALL: A Turkel–Zwas explicit large time-step Fortran program for solving the shallow-water equations in spherical coordinates. *Comput. Geosci.*, **17,** 1311–1343.

Neta, B., 1988: The effect of spatial discretization on the steady-state solution of the shallow-water equations. *Proc. Int. Conf. on* Computational Methods on Flow Analysis, Okayama, Japan, 111–118.

——, 1989: Analysis of the Turkel–Zwas scheme for the shallow-water equations. *IMACS Transactions on Scientific Computing: Numerical and Applied Mathematics,* W. F. Ames, Ed., J. C. Balzer AG, Scientific Publ. Co., 257–264.

——, and C. L. DeVito, 1988: The transfer function analysis of various schemes for the two-dimensional shallow-water equations. *Comput. Math. Appl.*, **16,** 111–137.

——, and I. M. Navon, 1989: Analysis of the Turkel–Zwas scheme for the shallow-water equations. *J. Comput. Phys.*, **81,** 277–299.

——, and R. T. Williams, 1989: Rossby wave frequencies and group velocities for finite element and finite difference approximations to the vorticity-divergence and the primitive forms of the shallow water equations. *Mon. Wea. Rev.*, **117,** 1439–1457.

Schoenstadt, A. L., 1977: The effect of spatial discretization on the steady-state and transient solutions of a dispersive wave equation. *J. Comput. Phys.*, **23,** 364–379.

——, 1980: A transfer function analysis of numerical scheme used to simulate geostrophic adjustment. *Mon. Wea. Rev.*, **108,** 1248–1259.

Trefethen, L. N., 1982: Group velocity in finite difference schemes. *SIAM Rev.*, **24,** 113–136.

Turkel, E., and G. Zwas, 1979: Explicit large-time-step schemes for the shallow-water equations. *Proc. Third Int. Symp. in Advances in Computer Methods for Partial Differential Equations,* Bethlehem, PA, IMACS, 65–69.

Wajsowicz, R. C., 1986: Free planetary waves in finite-difference numerical models. *J. Phys. Oceanogr.*, **16,** 773–789.

Winninghoff, F. J., 1968: On the adjustment toward a geostrophic balance in a simple primitive equation model with application to the problem on initialization and objective analysis. Ph.D. thesis, University of California, Los Angeles, 161 pp.